Radiation closure and diurnal cycle of the clear-sky dust instantaneous direct radiative forcing over Arabian Peninsula

Sergey Osipov(1), Georgiy Stenchikov(1), Helen Brindley(2), and Jamie Banks(2)
(1) Division of Physical Sciences and Engineering, King Abdullah University of Science and Technology, Thuwal, Saudi Arabia
(2) Space and Atmospheric Physics Group, Imperial College London, UK

Motivation

- Dust Direct Radiative Forcing (DRF) over the Arabian Peninsula is very large, as it is a major source of aerosol
- Improved quantification of dust radiative forcing over the Arabian Peninsula is required for regional and global climate studies, as well as for better understanding of the impact of dust on the Red Sea
- Arabian Peninsula is less studied compared to North Africa and lacks in-situ observations, so uncertainty in DRF are large

Model

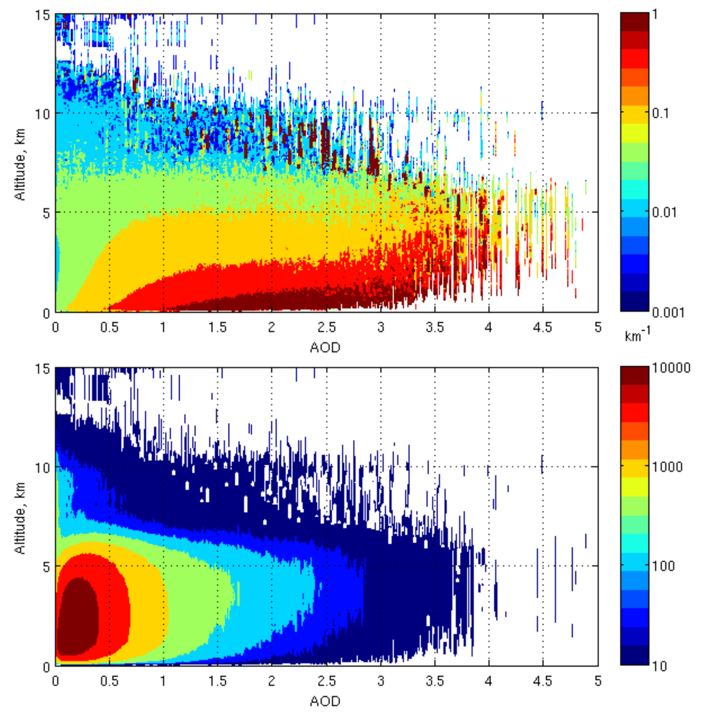

Fig. 1. Extinction profile of the dust at 532 nm (top panel) and corresponding number of samples (bottom panel) as a function of column AOD, derived from CALIPSO Lidar Level 2 Aerosol Profile product. Extinction profiles were screened over the Arabian Peninsula (land) and combined into column AOD bins with 0.01 step. Values, averaged within each bin, are color coded using the log-scale.

We have developed a standalone column radiation transport model coupled with the Mie calculations and driven by ECMWF reanalysis meteorological fields and atmospheric composition from Global Modeling Initiative chemistry and transport model. As a radiative transfer core in this study we use the Rapid Radiative Transfer Model (RRTM). According to CALIPSO, the ratio of the "not dust" and "dust" successful retrievals (screened) in the column between 0 and 5 km is 2.04 percent. Hence, not surprisingly, dust is a dominant aerosol type over the Arabian Peninsula. We used Balkanski et al. (2007) refractive indices (RIs) of the mineral dust internally mixed with 0.9%, 1.5% and 2.7% volume weighted hematite to calculate aerosol optical properties (referred to as B09, B15 and B27 respectively). To define aerosol size distribution we use effective radius and standard deviation of the fine and coarse modes from Aeronet inversion products.

Model validation & Radiation closure

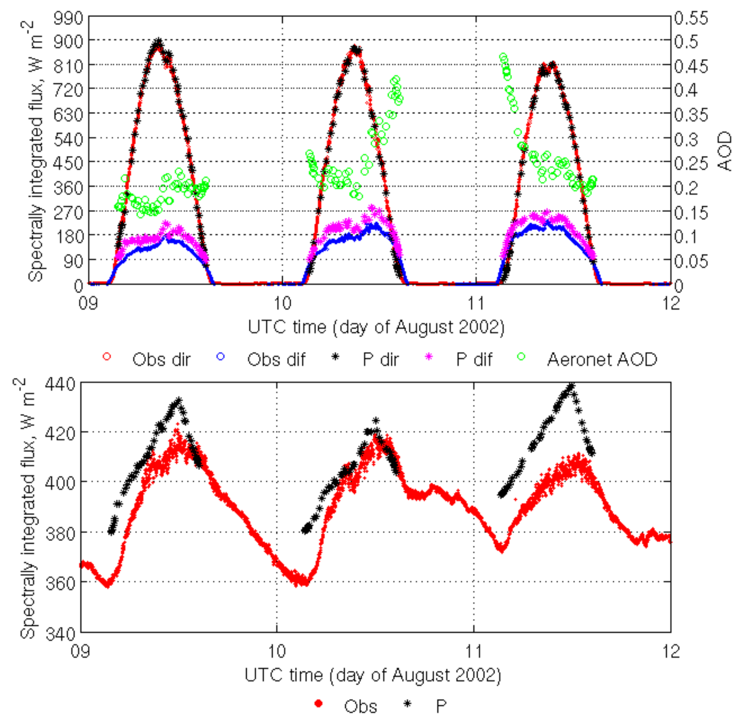

In order to validate model we carried out radiation closure for two specific locations: in the central Arabian desert at Solar Village and in the semi-desert area at the coastal plain of KAUST campus. For the first case measurements of the incident and upward fluxes are available (Fig. 2, 4). They were used to estimate broadband surface albedo and compare it (Fig. 3) with the one derived from the model runs based on the MODIS BRDF/Albedo product (Fig. 7). Table 1 provides comparison summary of the computed and observed fluxes. The second case study deals with a major dust outbreak that occurred over the Arabian Peninsula during March 2012.

Fig. 2. Surface downwelling fluxes at Solar village. SW surface downwelling perturbed experiment direct (P dir, black stars) and diffuse (P dif, purple stars), in-situ measured direct (Obs dir, red circles) and diffuse (Obs dif, blue circles) fluxes and Aeronet SDA column AOD at 500 nm (green, right vertical axis) are provided in the top panel. LW surface downwelling perturbed experiment (P, black stars) and in-situ measured (Obs, red circles) fluxes are provided it the bottom panel.

For KAUST case we also compared modeled TOA DRFs to those independently derived from GERB (Fig. 6). RMSE is 26 W m^{-2} and 7 W m^{-2}, while estimated GERB DRF error is +/- 15 W m^{-2} in SW and LW. The impact of LW scattering is critical in this case (RMSE is 7 W m^{-2}) with maximum error on 19 March reaching almost 16 W m^{-2}.

fluxes	direct down BOA	diffuse down BOA	up BOA	up TOA
SW model SW instrument	10 Wm^{-2} / 1.9% 2% at 1 kWm^{-2}	37 Wm^{-2} / 20% 3% at 1 kWm^{-2}	19 Wm^{-2} / 8.2% 3% at 1 kWm^{-2}	21 Wm^{-2} / 6.5% 5.1%
LW model LW instrument		3+14 Wm^{-2} / 4.1% +/- 10 Wm^{-2}	0 Wm^{-2} (25 Wm^{-2} / 4.5%) +/- 10 Wm^{-2}	19 Wm^{-2} / 1.8% 1.8%

Table 1. Comparison of the computed and observed fluxes at Solar Village. First line in each cell contains absolute and relative RMSE. Second line in each cell contains instrument uncertainty.

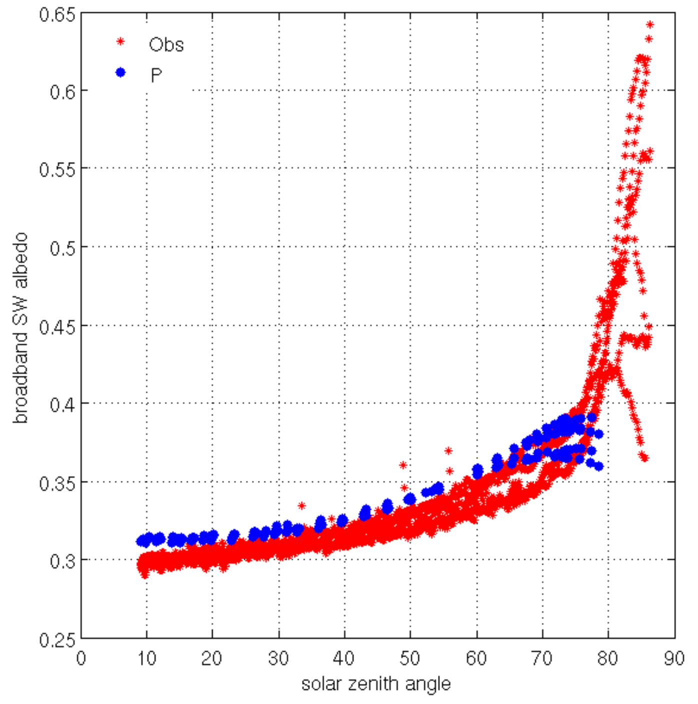

Fig. 3 (top). Three days accumulated broadband SW albedo at Solar village derived from ground-based measurements (Obs, red stars) and perturbed experiment based on MODIS BRDF (P, blue circles).

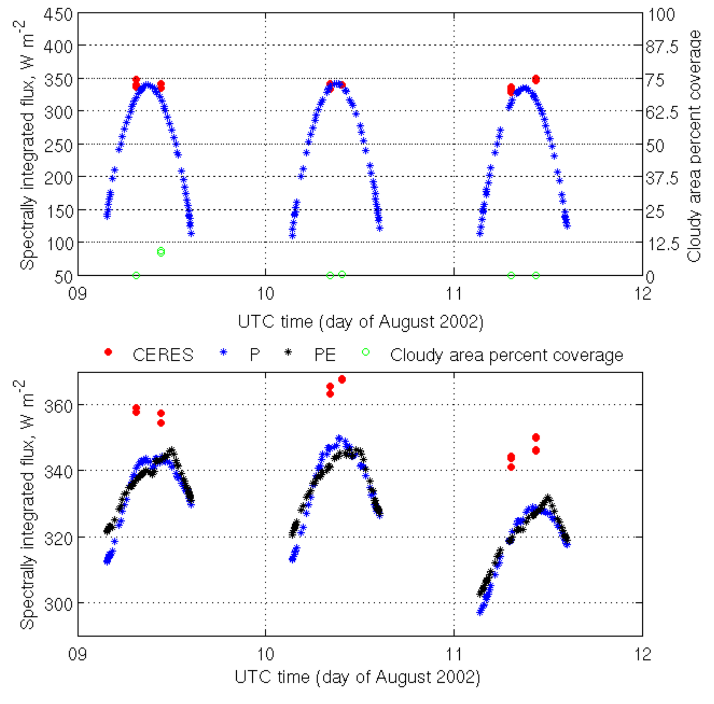

Fig. 5 (top). SW (top panel) and LW (bottom panel) computed with approximated surface temperature (P, blue) and prescribed from ERA-Interim (PE, cyan) and satellite inferred (CERES, red) TOA upwelling fluxes at Solar village. Cloudy area percent coverage derived from CERES product (top panel, green) is plotted against right vertical axis.

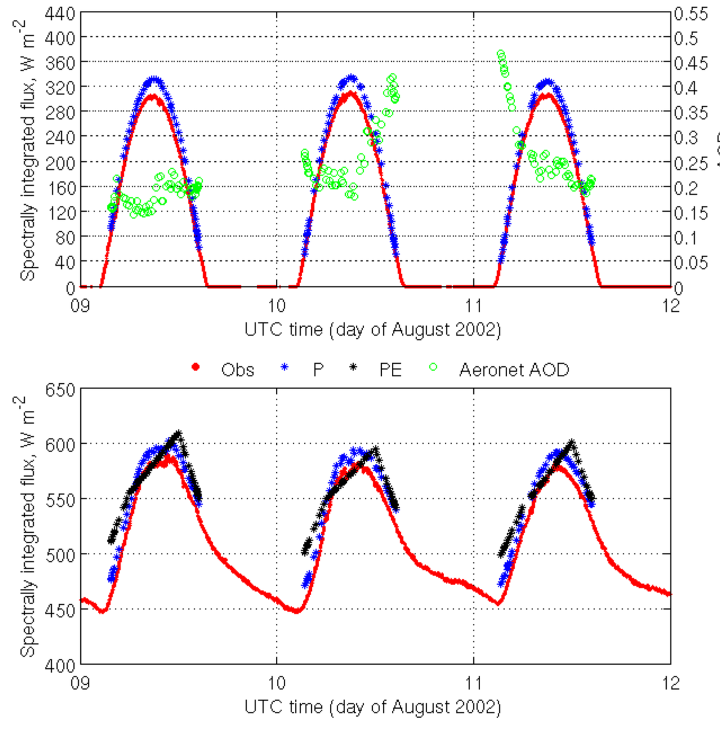

Fig. 4 (top). SW (top panel) and LW (bottom panel) computed surface upwelling fluxes with approximated surface temperature (P, blue) and prescribed from ERA-Interim (PE, black) and in-situ measurements (Obs, red) at Solar village. Aeronet SDA column AOD at 500 nm (top panel, green) is plotted against right vertical axis.

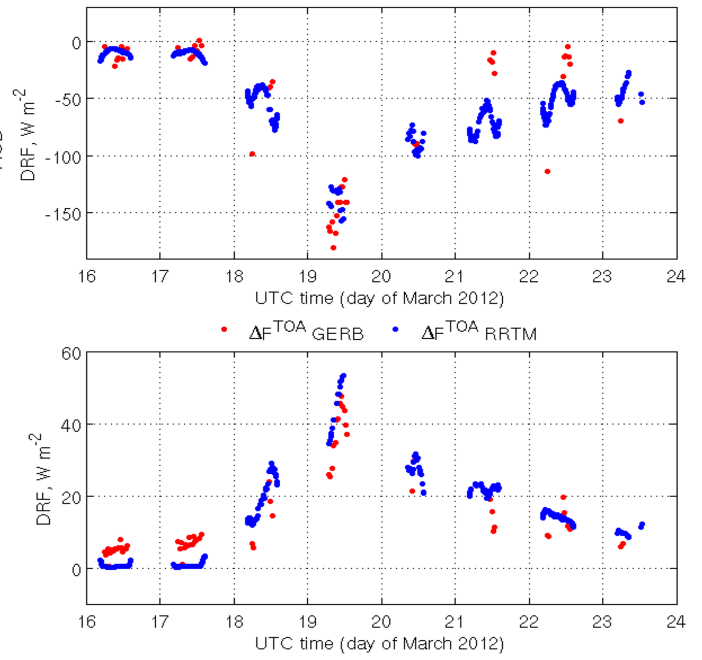

Fig. 6 (top). SW (top panel) and LW (bottom panel) TOA DRF at KAUST derived from model (RRTM, blue) and satellite retrieval (GERB, red).

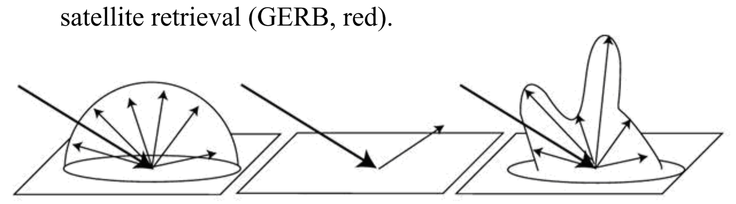

Fig. 7 (top). Schematic depiction of the (left to right) Lambertian reflectance, specular reflection and BRDF.

Diurnal cycle of SW TOA DRF

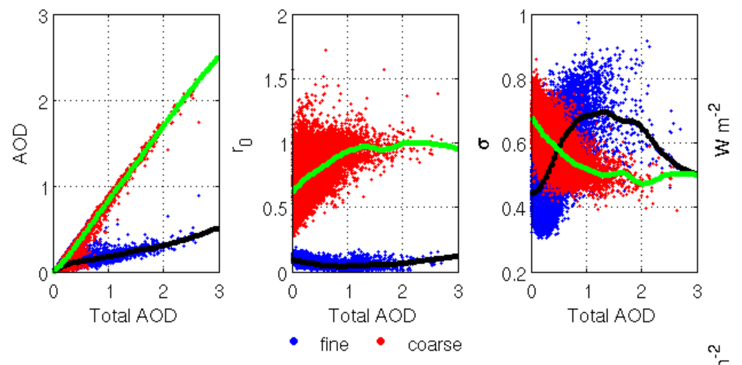

Fig. 8 (top). Fine (blue) and coarse (red) mode AOD (left panel) at 674 nm, median diameter r_0 (middle panel) and standard deviation σ (right panel) derived from Aeronet Inversion Level 2.0 product over the Arabian Peninsula. Thick lines indicate fitted values of the fine (black) and coarse (green) mode values used in sensitivity calculations.

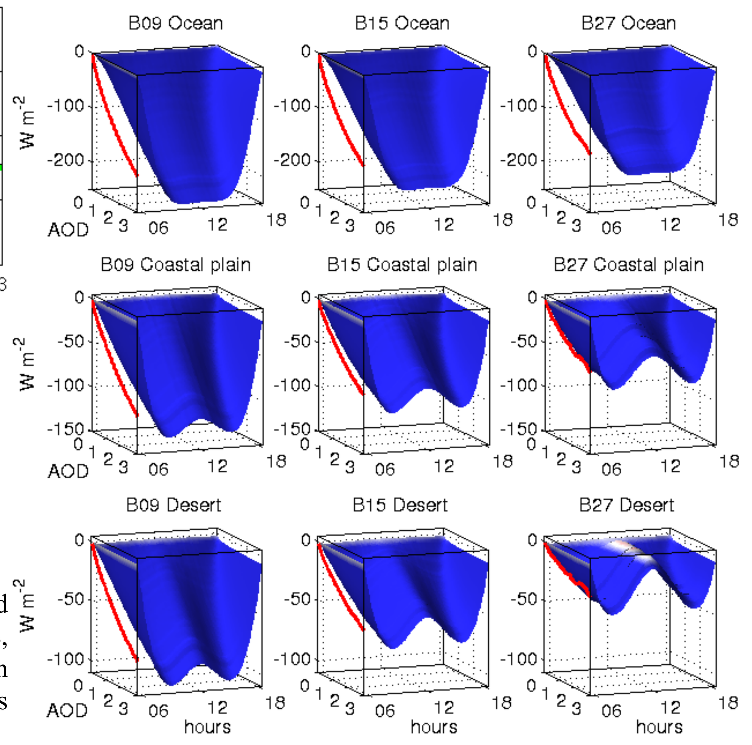

Fig. 9 (right). SW TOA DRF over ocean, coastal plain and desert surface albedo (top to bottom) for Balkansky 0.9%, 1.5% and 2.7% RIs (left to right) as a function of column AOD and local daytime (hours). Mean local daytime values (red) are projected on the DRF-AOD plane.

In Fig. 9 the simulated TOA forcing for the ocean case (top row) exhibits a relatively simple pattern with time of day. The magnitude of the forcing gets weaker with enhanced aerosol absorption (left to right). As the surface gets more reflective (top to bottom), the forcing is weakened and goes from being relatively flat during local noon to exhibiting a symmetrical weakening around local noon. The contrast between peak forcing and this localised reductions (min-max-min structure, MMM) becomes more exacerbated with increased aerosol absorption and surface albedo, such that the maximum difference in forcing between morning/evening and local noon is seen for the most absorbing aerosol over the desert surface (bottom right panel). For this case the sign of the forcing switches from negative to positive and then again to negative through the course of the day, indicating a SW cooling-heating-cooling of the Earth-atmosphere system. These results are consistent with those derived observationally by Ansell et al. (2014) and Banks et al. (2014) over northern Africa.

Detailed process analysis revealed that:

- Anisotropic scattering by dust significantly contributes to the diurnal cycle of the TOA and BOA DRF and explains the MMM structure.
- Higher surface albedo modulates ΔF^{TOA} , ΔF^{BOA} , and ΔF^{A} and shifts them towards the positive bound.
- Stronger absorption by dust significantly contributes to the diurnal cycle of the ΔF^{A}. It also shifts ΔF^{TOA} and ΔF^{A} towards the positive bound but has opposite effect on ΔF^{BOA}

Effect of the surface albedo on DRF

Experimental and theoretical studies have shown the dependence of the surface albedo on the solar zenith angle, ratio of the direct and diffuse fluxes and, in case of ocean surface, on wind speed (or surface roughness) and chlorophyll concentration (Lyapustin, 1999; Li et al., 2006; Jin et al., 2004). Using the MODIS Bidirectional Reflectance Distribution Function (BRDF) /Albedo product MCD43 (based on the RossThickLiSparce-Reciprocal model) total albedo in SW is given by a weighted sum of black-sky (q_{bsa}, direct radiation) and white-sky (q_{wsa}, diffuse radiation) albedos:

$$q(\lambda,\theta) = \frac{q_{bsa}(\lambda,\theta)F^{dir} + q_{wsa}(\lambda)F^{dif}}{F^{dir}+F^{dif}}$$

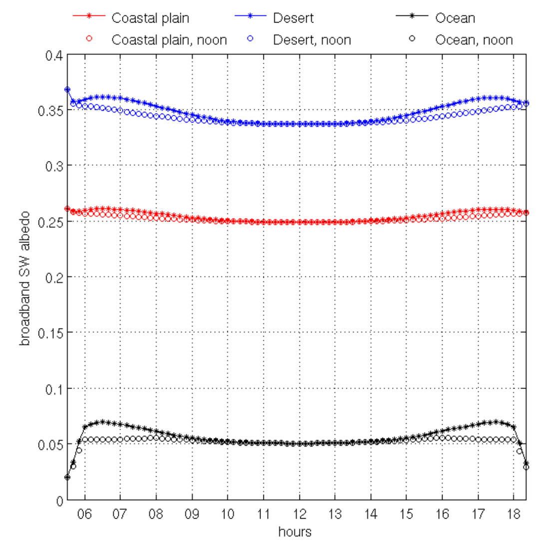

Fig. 10 (left). Broadband SW albedo for desert (blue), coastal plain (red) and ocean (black) with diurnal cycle (lines with stars) and fixed solar zenith angle (circles) averaged over the range of considered optical depths.

The difference δF of the forcings calculated with the varying albedo q and the fixed albedo $q_{fixed}=q(\theta=\theta_{noon}, r)$.

$$\delta F = \Delta F(\theta,\tau,q(\theta,r)) - \Delta F(\theta,\tau,q(\theta=\theta_{noon},r))$$

Fig. 10 shows broadband albedo diurnal cycles at the desert, coastal plain, and ocean. During the local solar noon q and q_{fixed} coincide exactly (by construction), but they deviate as the solar zenith angle grows due to variations of diffuse-to-direct flux ratio r . Fig. 11 shows corresponding contribution to the SW TOA DRF associated with diurnal cycle of q compared to q_{fixed}.

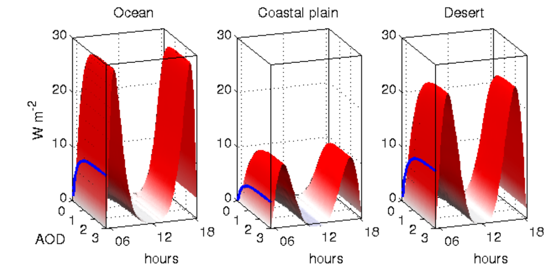

Fig. 11 (left). Contribution δF of the albedo diurnal cycle to the TOA SW DRF over ocean, coastal plain and desert (left to right) assuming Balkansky 1.5% refractive index as a function of column AOD and local daytime (hours). Mean local daytime values (blue) are projected on the DRF-AOD plane.

Daily mean DRF

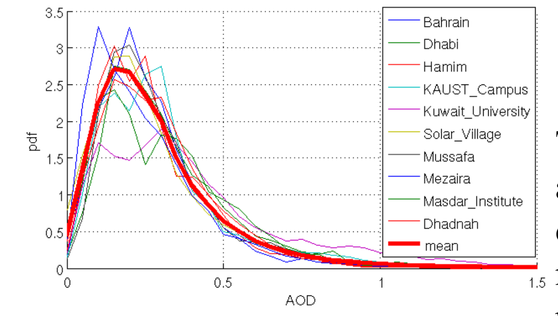

Fig. 12 (top). AOD at 675 nm pdf derived from Aeronet AOT Level 2.0 product over Arabian Peninsula. Thick red line indicate mean distribution that were used to derive the dust IDRF estimates.

The IDRF depends on optical depth quite non-linearly (Fig. 9) and therefore deriving mean IDRF from mean aerosol optical depth only might not always be accurate. To obtain the daily mean DRF we use AOD statistics. Fig. 12 shows the AOD probability density function (pdf, f(τ)) derived from Aeronet AOT Level 2.0 product. Sampling includes stations from the west and east coast and from the middle of the Arabian Peninsula with at least two years of observations. Daily mean dust DRF (Fig. 13) is computed using the distribution f(τ) as following:

$$\overline{\Delta F} = \frac{1}{T}\int_0^T \int_0^\infty \Delta F(\tau,t) f(\tau) d\tau dt$$

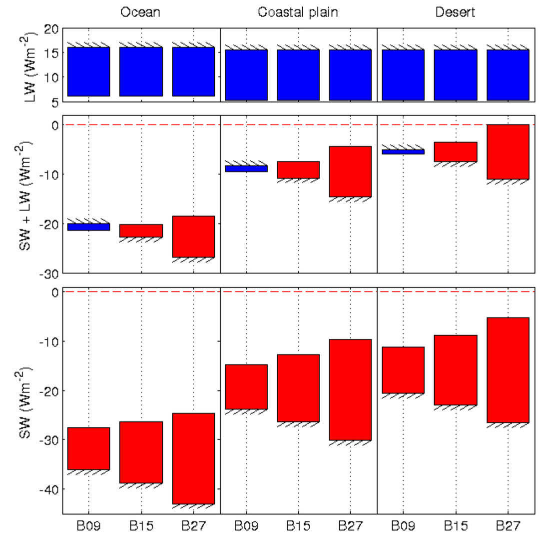

Fig. 13 (left). Daily mean dust DRF for B09, B15 and B27 RI (indicated by the vertical dash line in each column) and ocean, coastal plain and desert (left to right) surface albedo over the Arabian Peninsula. Each bar represents three diagnostic variables: ΔF^{TOA} , ΔF^{BOA} and ΔF^{A}. Hatching indicates the ΔF^{BOA} edge and thus the opposite edge is ΔF^{TOA}. The height of the bar corresponds to the absolute value of the atmospheric absorption due to dust or $|\Delta F^{A}|$ and color indicates the sign of the ΔF^{A} (blue for negative or cooling, red for positive or warming). LW, SW values and their sum are shown in the top, bottom and the middle rows respectively. Total column AOD used in calculations is 0.5 at 674 nm.

Conclusions

- Dust is a dominant aerosol over the Arabian Peninsula. The dust coarse mode contributes to the total column AOD more than the dust fine mode, and has to be correctly represented in modeling studies.
- The developed column aerosol-radiation model allows to comprehensively evaluate the dust optical characteristics and to obtain a relatively accurate radiation closure.
- The calculated radiation fluxes are in a good agreement with best available observations.
- Dust TOA DRF is estimated and compares well to the independently derived satellite values.
- The dust TOA DRF exhibit diurnal changes with three extrema structure over all considered surfaces, but dust TOA DRF diurnal cycle is the most pronounced over desert.
- Anisotropic scattering by dust significantly contributes to the diurnal cycle of the SW TOA and BOA DRF.
- Diurnal changes of the surface albedo, associated with the solar zenith angle and amount of diffuse radiation, has a strong impact on the dust DRF diurnal cycle and has to be explicitly accounted for in models.